AMERICAN SOCIETY FOR MICROBIOLOGY | Molecular and Cellular Biology®

RESEARCH ARTICLE

Truncated Adenomatous Polyposis Coli Mutation Induces Asef-Activated Golgi Fragmentation

Sang Bum Kim,[a]* Lu Zhang,[a]* Jimok Yoon,[b] Jeon Lee,[a] Jaewon Min,[a] Wenlin Li,[c] Nick V. Grishin,[c] Young-Ah Moon,[d] Woodring E. Wright,[a] Jerry W. Shay[a]

[a]Department of Cell Biology, University of Texas Southwestern Medical Center, Dallas, Texas, USA
[b]Department of Neuroscience, University of Texas Southwestern Medical Center, Dallas, Texas, USA
[c]Department of Biophysics and Biochemistry, University of Texas Southwestern Medical Center, Dallas, Texas, USA
[d]Department of Molecular Medicine, Inha University College of Medicine, Nam-gu, Incheon, Republic of Korea

ABSTRACT Adenomatous polyposis coli (APC) is a key molecule to maintain cellular homeostasis in colonic epithelium by regulating cell-cell adhesion, cell polarity, and cell migration through activating the APC-stimulated guanine nucleotide-exchange factor (Asef). The APC-activated Asef stimulates the small GTPase, which leads to decreased cell-cell adherence and cell polarity, and enhanced cell migration. In colorectal cancers, while truncated APC constitutively activates Asef and promotes cancer initiation and progression, regulation of Asef by full-length APC is still unclear. Here, we report the autoinhibition mechanism of full-length APC. We found that the armadillo repeats in full-length APC interact with the APC residues 1362 to 1540 (APC-2,3 repeats), and this interaction competes off and inhibits Asef. Deletion of APC-2,3 repeats permits Asef interactions leading to downstream signaling events, including the induction of Golgi fragmentation through the activation of the Asef-ROCK-MLC2. Truncated APC also disrupts protein trafficking and cholesterol homeostasis by inhibition of SREBP2 activity in a Golgi fragmentation-dependent manner. Our study thus uncovers the autoinhibition mechanism of full-length APC and a novel gain of function of truncated APC in regulating Golgi structure, as well as cholesterol homeostasis, which provides a potential target for pharmaceutical intervention against colon cancers.

KEYWORDS adenomatous polyposis coli, APC, armadillo repeats, Asef, Golgi fragmentation

The tumor suppressor adenomatous polyposis coli (APC) is highly mutated in sporadic and familial colorectal cancer (CRC) (1). Most somatic APC mutations occurs in the "mutation cluster region," and these typically result in the generation of truncated APC proteins that lack binding site for axin, β-catenin, microtubules, and EB1 (2, 3). Loss of microtubule binding properties of APC leads to defects in microtubule stabilization, actin nucleation, and directional migration (4–6). While loss of tumor suppressive function of APC by mutations is believed to be the earliest change in CRC tumorigenesis, increasing evidence suggest that truncated forms of APC protein may have gain-of-function properties such as in cell proliferation, cell survival, chromosomal instability, migration, and ultimately promoting CRC tumorigenesis (4, 7–11). Armadillo repeat domain of APC interacts with the APC-stimulated guanine nucleotide exchange factor (Asef; also known as Rho guanine nucleotide exchange factor 4 [ARHGEF4]) and stimulates Asef activity, thereby regulating cell morphology and migration (12). A recent study showed that peptidomimetric inhibitors of APC-Asef interaction blocks colorectal cancer migration (13), indicating that the interaction between APC and Asef may be an attractive target for anticancer therapy. Interestingly, a recent study using

Received 16 March 2018 **Returned for modification** 2 May 2018 **Accepted** 31 May 2018

Accepted manuscript posted online 4 June 2018

Citation Kim SB, Zhang L, Yoon J, Lee J, Min J, Li W, Grishin NV, Moon Y-A, Wright WE, Shay JW. 2018. Truncated adenomatous polyposis coli mutation induces Asef-activated Golgi fragmentation. Mol Cell Biol 38:e00135-18. https://doi.org/10.1128/MCB.00135-18.

Address correspondence to Sang Bum Kim, ksbom1@yuhs.ac, or Jerry W. Shay, jerry.shay@utsouthwestern.edu.

* Present address: Sang Bum Kim, Severance Biomedical Science Institute, Yonsei University College of Medicine, Seoul, Republic of Korea; Lu Zhang, Oncology Discovery, AbbVie, Inc., North Chicago, Illinois, USA.

S.B.K. and L.Z. are co-first authors.

RNA interference showed that truncated APC mutation is required for regulation of the Asef-mediated cell migration (8). Knockdown of either Asef or APC results in a significant decreases in cell migration but only in truncated APC cell lines. In addition, overexpression of full-length APC did not increase Asef-mediated cell migration (8). Since truncations in APC is an early event in CRC initiation, unraveling novel functions/mechanisms of truncated APC in the regulation of Asef activity and cellular physiology are likely to be important to understand both cancer initiation and progression.

The Golgi apparatus is a highly dynamic cellular organelle, which functions in sorting and transport of proteins in the secretory pathway as well as in regulating posttranslational protein modifications. Reorientation of the Golgi structure toward the leading edge is critical for directional cell migration (14). A typical mammalian Golgi apparatus consists of a series of parallel, flattened, disk-shaped cisternae, which align into stacks. However, the Golgi complex is fragmented and dispersed when cells are exposed to cellular stressors such as DNA-damaging agents (15). Golgi fragmentation is also observed in several age-related diseases, including Alzheimer's disease, Parkinson's disease and cancer (16), suggesting that the Golgi apparatus may have important roles in the pathogenesis of a variety of human diseases. While Golgi fragmentation was first observed in cells by electron microscopy over 60 years ago, the mechanisms and significance of Golgi fragmentation in human diseases remain poorly understood.

Recently, we demonstrated that CRC cells with truncated APC harbor defects in SREBP2 feedback activation in response to a novel anti-CRC drug, TASIN-1 (7), suggesting that truncated APC proteins might also have a dominant role in cholesterol homeostasis. Activation of the SREBP pathway, which is the master regulator of sterol homeostasis, involves transport of SREBP from the endoplasmic reticulum (ER) to the Golgi apparatus by COPII vesicles, cleavage in the Golgi apparatus, and subsequent translocation into the nucleus (17, 18). Considering the critical role of Golgi apparatus in the regulation of the SREBP pathway and the dominant effects of truncated APC on SREBP feedback activation, we investigated the effects of truncated APC in Golgi organization and the underlying molecular mechanisms.

RESULTS

Truncated APC induces Golgi fragmentation. To investigate the effect of a truncated APC on Golgi organization in CRC cell lines, a Golgi matrix protein, GM130, was visualized in wild-type (WT) and truncated APC cell lines. Immunocytochemistry analysis revealed that WT APC cells (RKO and HCT116) had centralized more compact Golgi structure, whereas truncated APC cells (DLD1 and HT29) had more fragmented and scattered Golgi structures (Fig. 1A). To analyze Golgi fragmentation quantitatively, we developed an open source tool for Golgi image analysis. Using this graphical user interface (GUI)-based tool, we analyzed Golgi fragmentation taking the number of fragments, the area of fragments, and distances between the fragments as features of Golgi fragmentation and scattering (see Fig. S1 in the supplemental material). Quantitative analysis confirmed that the cells with fragmented Golgi structure had increases in both the number of Golgi fragments and the distance between Golgi fragments but an overall decrease in the area of Golgi fragments compared to cells with intact Golgi structure (Fig. 1B).

We also observed that CRC lines with WT APC (RKO and HCT116) or depletion in truncated APC (DLD1/shAPC) had intact Golgi structures, whereas the same cells with ectopic expression of truncated APC (RKO/A1309 and HCT116/A1309) or endogenous truncated APC (DLD1) exhibited more fragmented Golgi structures (Fig. 1C), indicating that truncated APC is essential for the Golgi fragmentation. To address which domain in truncated APC is critical for Golgi fragmentation, we next generated stable cell lines expressing different APC fragments, including APC 1-400 (A400), 1-900 (A900), and 1-1309 (A1309) amino acids. Expression of A900 and A1309 but not A400 induced Golgi fragmentation in DLD1/shAPC cells (Fig. 1D to F), indicating that armadillo repeats may be critical for Golgi fragmentation. Further immunohistochemical analysis showed that mouse colon crypts derived from the *CPC*; *Apc* mice (19) harboring truncated APC in the colonic epithelial cells exhibited fragmented and diffuse Golgi structures, whereas WT APC mice exhibited

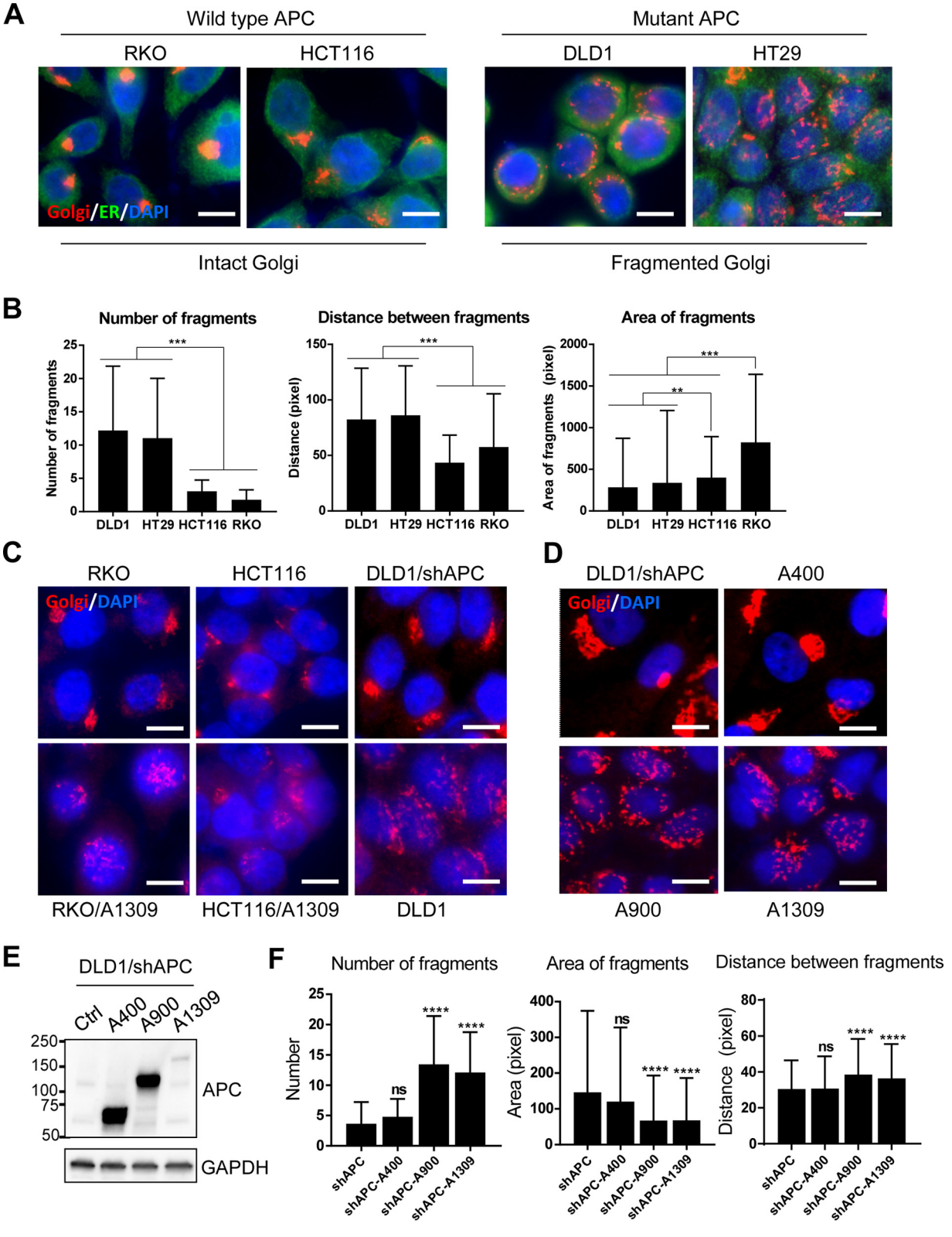

FIG 1 Truncated APC mutation is involved in Golgi fragmentation. (A) Immunostaining for a Golgi marker (GM130, red) and an ER marker (calnexin, green) in WT APC and mutant APC CRC cells. Scale bars, 10 μm. (B) Quantitative analysis of Golgi fragmentation. Truncated APC cells (DLD1 and HT29) show an increase in the number of fragments and distance between fragments but a decrease in the area of fragments. (C) Immunostaining for GM130 in isogenic CRC lines with or without truncated APC expression. Scale bars, 10 μm. (D) Immunostaining for GM130 in DLD1/shAPC cells and their isogenic derivatives expressing A400, A900, or A1309 fragments. Scale bar, 10 μm. (E) A Western blot shows the expression of APC fragments in stable cell lines. (F) Quantitative analysis of Golgi fragmentation in DLD1/shAPC cells and their isogenic derivatives expressing A400, A900, or A1309 fragments. **, $P < 0.01$; ***, $P < 0.001$; ****, $P < 0.0001$ (analysis of variance [ANOVA] test; $n > 50$ per group).

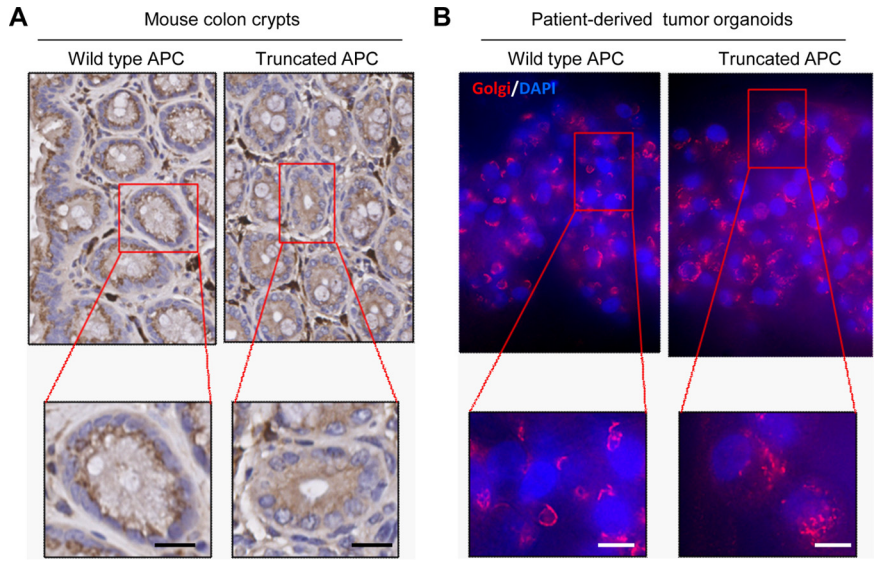

FIG 2 Truncated APC-induced Golgi fragmentation *in vivo*. (A) Immunohistochemistry for GM130 (brown) on mouse crypts derived from WT APC mice or *CPC;Apc* mice which have truncated APC in colon. Scale bars, 20 μm. (B) Immunostaining for GM130 (red) on human patient-derived CRC tumor organoids cultured in 3D Matrigel with WT or truncated APC. Scale bars, 10 μm.

more centralized intact Golgi structures in the crypt sections (Fig. 2A). We also observed the Golgi organization in early passage CRC patient-derived organoids (PDO). Patient-derived CRC tumors were grown in Matrigel for a short term and visualized with GM130 by immunostaining. The same phenotype was observed in CRC PDO (Fig. 2B) with WT (intact Golgi structure) or truncated APC (fragmented Golgi structure), indicating the *in vivo* relevance of these observations.

Golgi fragmentation is induced by APC-ARM but inhibited by APC-2,3 repeat. While APC fragments include armadillo repeat domain (ARM) that promotes Golgi fragmentation, ARM in full-length APC does not induce Golgi fragmentation, suggesting that there is an inhibitory mechanism in full-length APC. To understand the mechanism how APC regulates the Golgi structure, we generated various fragments of APC protein tagged with green fluorescent protein (GFP) (Fig. 3A) and expressed in APC WT cells (Fig. 3B). Golgi fragmentation is observed in the cells expressing APC-ARM (APC 334-900), APC900, and APC1309. However, expression of APC fragments including both ARM and APC residues 1362 to 1540, containing the second and third 20-amino-acid (APC-2,3) repeats (APC1572, APC1628, APC2500, and APC FL) did not induce Golgi fragmentation. Consistently, expression of APC FL which has a deletion of APC-2,3 repeats [APC(Δ2,3)] induced Golgi fragmentation, indicating that APC-2,3 repeats has inhibitory functions in ARM-induced Golgi fragmentation (Fig. 3B and C).

Golgi fragmentation is induced by Asef-ROCK-MLC2 pathway. A large number of the APC-interacting proteins bind to the ARM of APC. These include Asef, which is the Rho guanine nucleotide exchange factor (RhoGEF) that regulates the actin cytoskeleton, cell morphology, and polarity (12). While the expression of either APC334-900 or APC900 induced Golgi fragmentation, the expression of either APC334-900 (N507K) or APC900 (N507K), which has mutation in Asef interacting site (20, 21), prevented Golgi fragmentation (Fig. 4A), suggesting that Asef is the downstream target for truncated APC-induced Golgi fragmentation.

Asef regulates cell polarity and migration through Rho GTPases and is believed to contribute to aberrant migratory property of CRC cells harboring mutant APC (8). Several previous studies suggested that Asef cross-links between truncated APC and Rho GTPases in regulating cell polarity and migration (22, 23). Rho GTPases and Cdc42-MRCK (myotonic dystrophy kinase-related Cdc42-binding kinase) and Rho-ROCK (Rho kinase) signaling cooperatively regulate actomyosin dynamics through activation

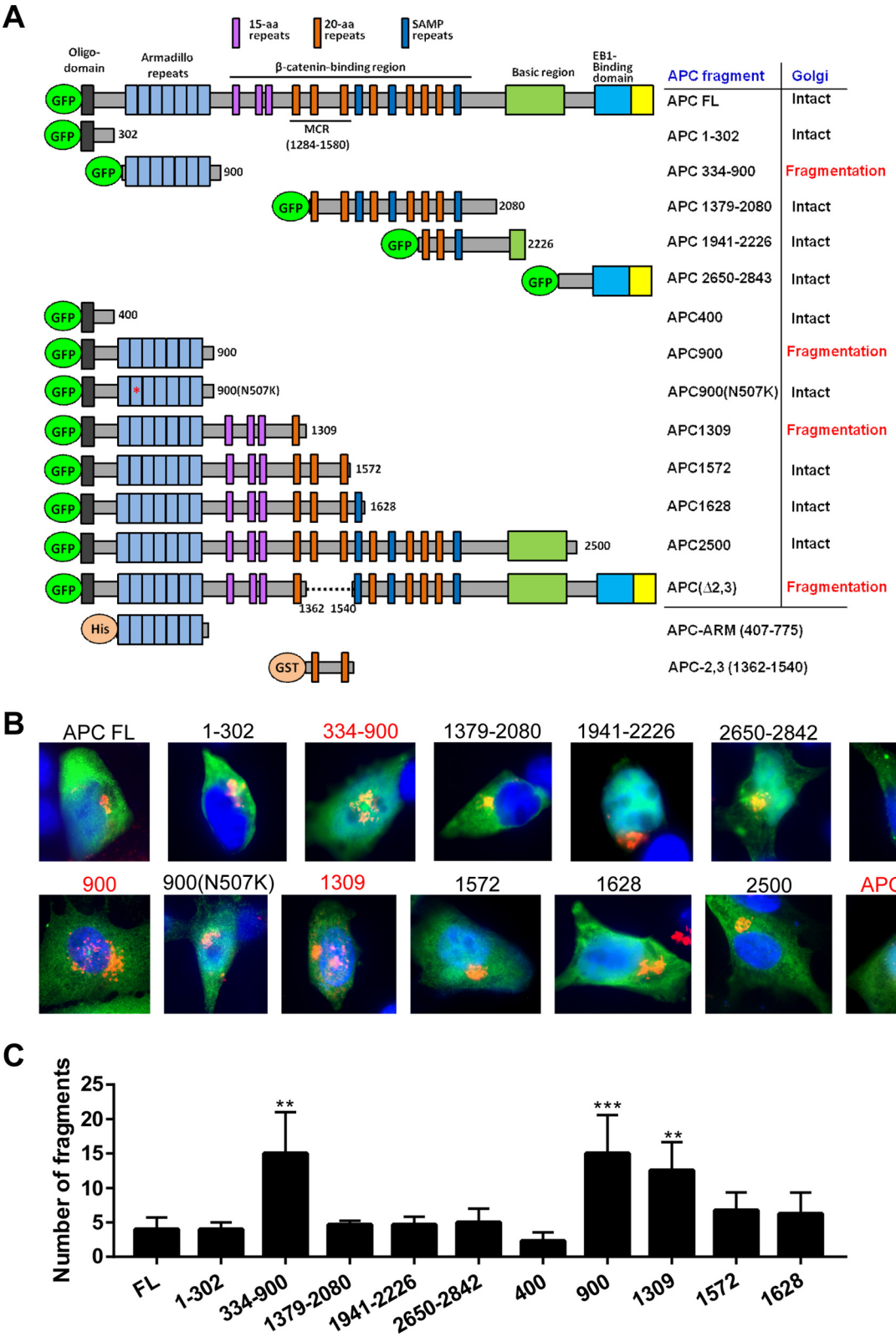

FIG 3 Armadillo repeats of APC positively affect Golgi fragmentation. (A) Schematic diagram of APC depicting domains present and different fragments used for this study. Numbers represent the amino acids. The table shows a summary for APC fragments and their effects on Golgi structure. (B) WT APC cells (HEK293) transfected with GFP-tagged APC fragments are indicated by green fluorescence. The structure of the Golgi complex was assessed using GM130 (red). The nucleus is represented in blue. APC fragments that induce Golgi fragmentation are indicated in red. (C) Quantitation of fragmented Golgi structure in cells expressing truncated APC proteins. **, $P < 0.01$; ***, $P < 0.001$ (compared to APC FL in ANOVA test).

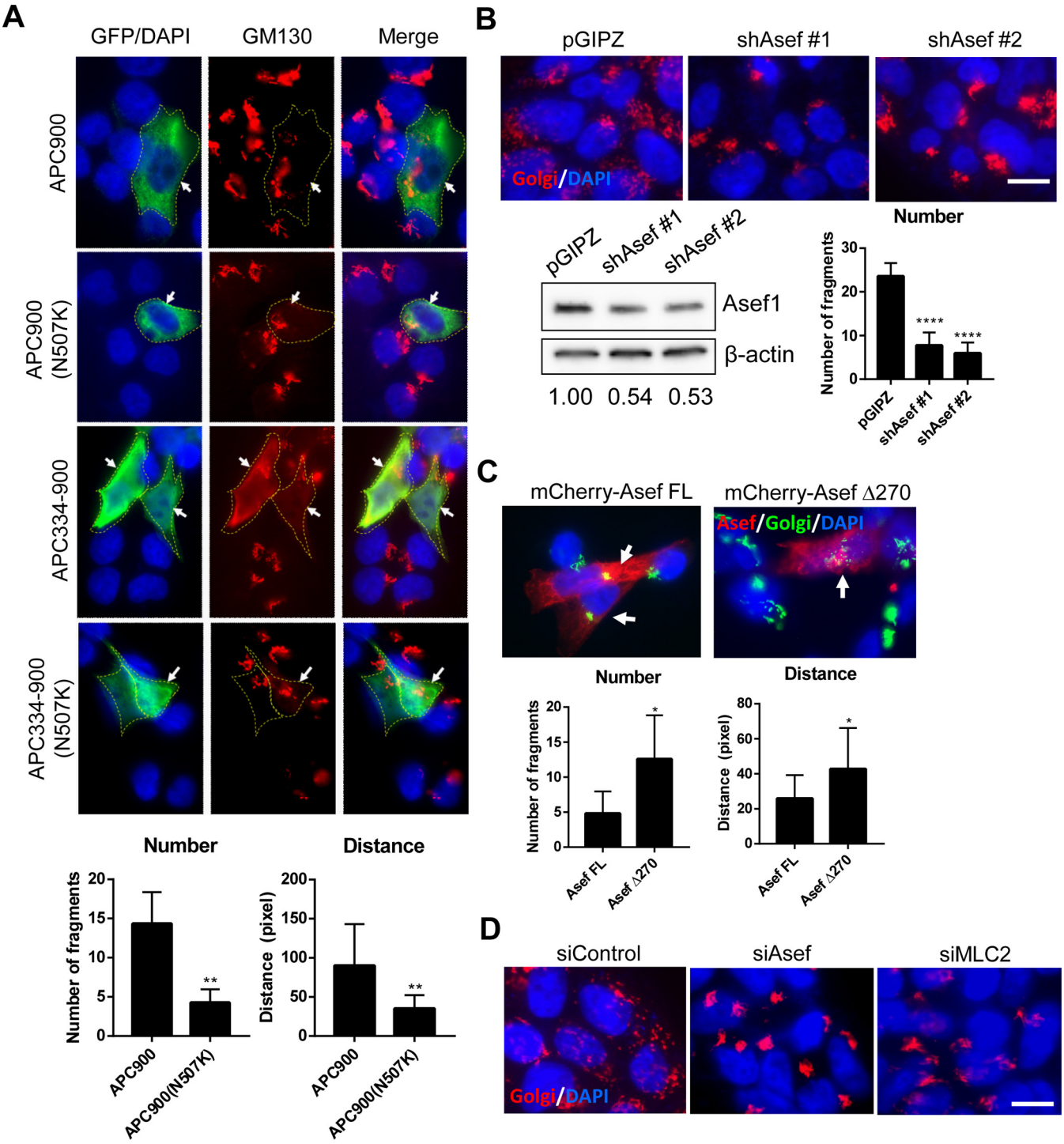

FIG 4 Mechanism of Golgi fragmentation by truncated APC. (A) HCT116 cells were transfected with GFP-APC900, GFP-APC900(N507K), GFP-APC334-900, or GFP-APC334-900(N507K) and stained for the Golgi structures (red) using GM130. The arrows indicate cells expressing GFP-tagged APC fragments (green). (B) Immunostaining for Golgi structures (red) in DLD1 cells infected with lentivirus expressing control (pGIPZ vector) or Asef shRNAs for stable Asef knockdown. Scale bar, 10 μm. The expression of Asef and quantitative Golgi fragmentation are shown below. (C) HCT116 cells were transfected with mCherry-Asef FL or mCherry-Asef(Δ270) (constitutively active form) and stained for the Golgi structures (green) using GM130. The arrows indicate cells expressing mCherry-tagged Asef proteins (red). (D) Immunostaining for GM130 in DLD1 cells transfected with control siRNA, Asef siRNA, or MLC2 siRNA for transient knockdown of Asef or MLC2. Scale bar, 10 μm. (E and F) Immunostaining for GM130 and pMLC2 and quantitative analysis of Golgi fragmentation in DLD1 cells treated with vehicle (control) or 10 μM ROCK inhibitor (Y27632). Scale bar, 10 μm. (G and H) Immunostaining for GM130 and quantitative analysis of Golgi fragmentation in DLD1 cells treated with vehicle (control) or 50 μM blebbistatin (Blebb). (I) Western blot for MYPT and MLC2 phosphorylation in DLD1 cells treated with or without 10 μM Y27632. (J) Western blot for MYPT and MLC2 phosphorylation in DLD1, DLD1/shAPC, and DLD1/shAPC cells expressing A400, A900, and A1309. (K) Western blot for MLC2 phosphorylation in DLD1, DLD1/shAPC, and DLD1/shAPC cells expressing A900 and A900(N507K).

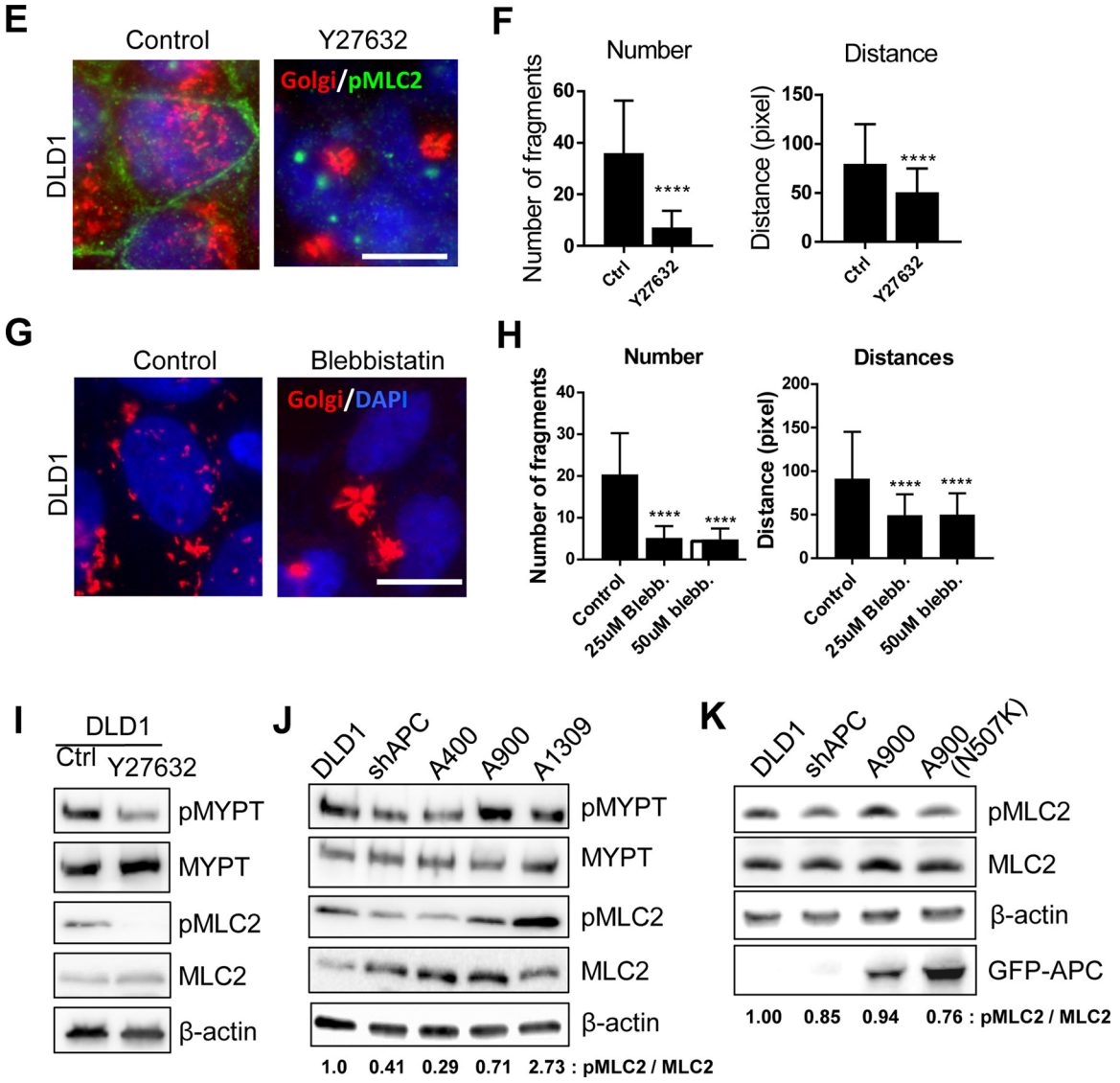

FIG 4 (Continued)

of myosin phosphatase (MYPT) and myosin light chain 2 (MLC2) (24). In addition, activation of myosin results in Golgi disorganization (25). Since the expression of APC900 (N507K) suppressed Golgi fragmentation (Fig. 4A), we further analyzed the effects of Asef in truncated APC-induced Golgi fragmentation.

Stable knockdown of Asef restored Golgi structure in DLD1 cells (Fig. 4B) and overexpression of full-length Asef (mCherry-Asef FL) maintains intact Golgi structure (Fig. 4C) in WT APC cells. However, the expression of constitutively active Asef (mCherry-AsefΔ270) induces Golgi fragmentation (Fig. 4C), which indicates that activation of Asef is sufficient to induce Golgi fragmentation. Transient knockdown of Asef or MLC2 using small interfering RNAs (siRNAs) also restored Golgi structure in DLD1 cells (Fig. 4D). Since treatment with the MRCK inhibitor (BDP5290) did not inhibit MYPT or MLC2 phosphorylation nor restore the Golgi structure in DLD1 cells (data not shown), we suggested that truncated APC induces Golgi fragmentation through activation of the Asef-RhoA-ROCK-MLC2 pathway. Small molecule inhibitors against ROCK (Y27632) and MLC2 inhibitor (blebbistatin) were used to investigate whether this pathway is critical for Golgi fragmentation in DLD1 cells. Inhibition of ROCK via Y27632 treatment (Fig. 4E and F) or MLC2 by blebbistatin treatment (Fig. 4G and H) in DLD1 cells restored

the intact Golgi structure. The ROCK inhibitor also reduced phosphorylation of MYPT and MLC2 in DLD1 cells (Fig. 4I). Depletion of truncated APC in DLD1 cells reduced MYPT or MLC2 phosphorylation which was not affected by expression of APC400 fragment. However, expression of APC900 or APC1309 in DLD1/shAPC cells induced MYPT and MLC2 phosphorylation (Fig. 4J). While expression of APC900 in DLD1/shAPC induced MLC2 phosphorylation, the expression of APC900 (N507K) did not induce MLC2 phosphorylation (Fig. 4K), also supporting that truncated APC induces MYTP and MLC2 phosphorylation through Asef interaction. These data can be interpreted to indicate that the Asef-ROCK-MLC2 pathway is critical for truncated APC-induced Golgi fragmentation.

Full-length APC regulates Asef activity by autoinhibition. Previously, we showed that the ARM in truncated APC constitutively activates Asef and promotes Golgi fragmentation. However, ARM in APC fragments containing APC-2,3 repeats (APC FL, APC1572, or APC1628) did not induce Golgi fragmentation. In contrast, APC FL which has a deletion of APC-2,3 repeats [APC(Δ2,3)] induced Golgi fragmentation (Fig. 3 and Fig. 5A), suggesting that there is an inhibitory mechanism in APC-2,3 repeats. In most truncated APC mutations, APC-2,3 repeats are deleted (26). Previous crystal structure analyses showed that the ARM in β-catenin interacts with APC-2,3 repeats (26). Similar to the β-catenin-ARM, APC-ARM also forms a right-handed superhelix, with each repeat consisting of three α-helices (H1, H2, and H3) packing extensively (20). Sequencing alignment of APC-ARM and β-catenin-ARM shows that both ARMs have consensus patterns of core residues of H1, H2, and H3 helices (see Fig. S2 in the supplemental material); therefore, we can predict the APC-2,3 repeats binding site on APC-ARM (Fig. 5B, green). When we compared the predicted APC-2,3 binding sites and already published Asef binding site in APC-ARM, we found that APC-ARM shares key residues for interaction with APC-2,3 (green highlight) and Asef (red highlight) (20) (Fig. 5B), suggesting that APC-2,3 can inhibit interactions between the APC-ARM and Asef by direct binding to APC-ARM. To address whether APC-ARM interacts with APC-2,3, we first purified His-tagged APC-ARM and glutathione *S*-transferase (GST)-tagged APC-2,3 proteins and performed *in vitro* binding assays. As shown in Fig. 5C and D, APC-ARM can be pulled down by APC-2,3. We also found that APC-ARM can be pulled down by biotin-tagged Asef (APC binding region) peptide. However, addition of APC-2,3 repeats reduced the interaction between biotin-Asef(ABR) and the APC-ARM in a concentration dependent manner (Fig. 5E and F). To validate this observation in cells, Flag-tagged APC-2,3 repeats were ectopically expressed in DLD1 cells. DLD1 cells expressing APC-2,3 repeats (DLD1/APC-2,3) exhibited more centralized Golgi structures (Fig. 5G and H). Expression of APC-2,3 in DLD1 cells also reduced MYPT and MLC2 phosphorylation (Fig. 5I). Thus, in WT APC cells, the N terminus of the APC protein folds back through interaction between the armadillo domain and the APC-2,3 region, competing off Asef thereby inactivating the downstream pathway. Deletion of APC-2,3 repeats in APC FL (APCΔ2,3) shows stronger interaction with Asef compared to APC FL (Fig. 5J) supporting this hypothesis. To determine whether the interaction between Asef and APC(Δ2,3) enhances Asef activity, we pulled down active Asef using RhoA-G17A–agarose beads, which are designed to pull down only the active form of RhoA-GEF (Fig. 5K). We also confirmed that while expression of APC900 in DLD1/shAPC cell increased active RhoA (GTP form), expression of APC-2,3 decreased active RhoA in DLD1 cells by rhotekin-RBD pulldown assay (Fig. 5L and M). To conclude, in CRC cells harboring truncated APC, the APC-2,3 region that is important for armadillo repeats interaction is absent, releasing the armadillo repeats to bind and activate Asef and the downstream RhoA-ROCK-MLC pathway, leading to Golgi fragmentation (Fig. 6).

Golgi fragmentation modulates cholesterol homeostasis. A major function of the Golgi apparatus is its role in protein trafficking. To observe effects of Golgi fragmentation in secretory trafficking, the secretion of secreted embryonic alkaline phosphatase (SEAP) was monitored over time in the presence and absence of truncated APC in DLD1 cells expressing pSelect-zeo-SEAP plasmid. Knockdown of truncated APC in DLD1 cells

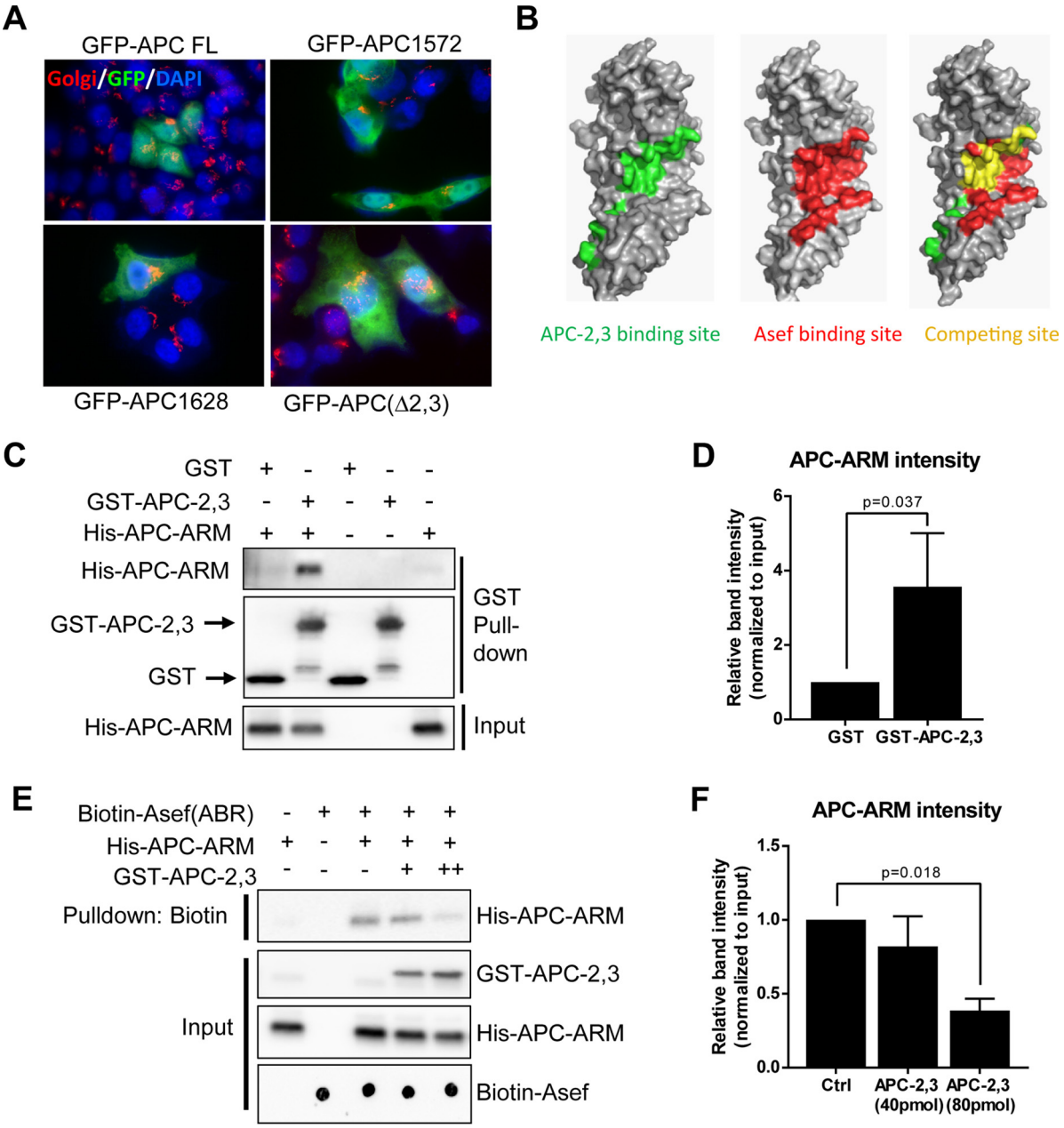

FIG 5 Full-length APC controls Asef activity by autoinhibition. (A) HCT116 cells were transfected with GFP-APC FL, APC1572, APC1628, or APC(Δ2,3) and stained for the Golgi structures (red) using GM130. Cells expressing GFP-tagged APC fragments are indicated by green fluorescence. Nuclei are represented in blue. (B) Predicted APC-2,3 repeats binding site on APC-ARM is indicated in green. Red highlights indicate key residues for Asef interaction. Shared key residues for interaction with APC-2,3 and Asef are highlighted in yellow. (C) A GST pulldown assay indicates that APC-2,3 directly interacts with APC-ARM *in vitro*. (D) Quantitative data for APC-ARM intensity from triplicate GSTpulldown experiments. (E) Biotin pulldown assay shows that biotin-Asef (ABR) peptide interacts with APC-ARM. However, APC-2,3 fragments compete off the interaction between Asef(ABR) and APC-ARM in a dose-dependent manner. (F) Quantitative data for APC-ARM intensity from triplicate biotin pulldown assays. (G and H) Immunostaining for GM130 and quantitative analysis of Golgi fragmentation in DLD1 cells expressing empty vector or APC-2,3 fragment. Scale bar, 10 μm. (I) Western blot for MYPT and MLC2 phosphorylation in DLD1 cells expressing empty vector or APC-2,3 fragment. (J) HCT116 cells were cotransfected with mCherry-Asef and GFP-APC FL or mCherry-Asef and GFP-APC(Δ2,3). mCherry pulldown shows interaction between Asef and APC, and RhoA-G17A pulldown shows active Asef which interacts with RhoA. (K) A pulldown assay using RhoA-G17A shows active Asef in the cells expressing truncated APC proteins. (L and M) A pulldown assay using rhotekin-RBD shows active RhoA (GTP form) in the cells expressing truncated APC or APC-2,3 fragments.

showed enhanced SEAP secretion compared to DLD1 cells, which was not affected by nocodazole treatment but inhibited by brefeldin A (BFA) treatment (Fig. 7A), suggesting that microtubules are not involved in truncated APC-induced trafficking impairment. Next, to observe whether truncated APC-induced Golgi fragmentation eliminates the

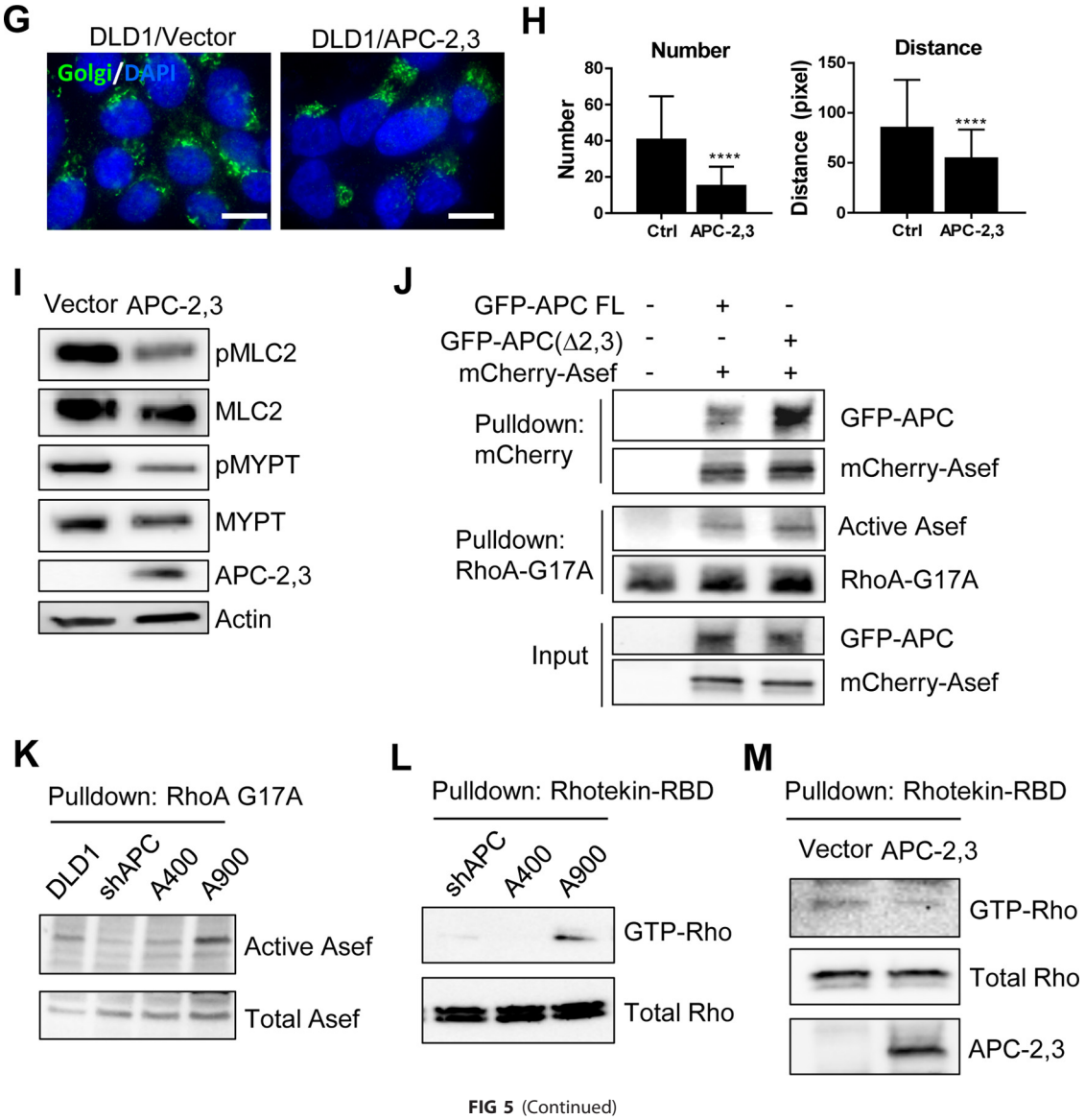

FIG 5 (Continued)

spatial distinction between ER and Golgi structures, we performed costaining with the Golgi apparatus (GM130) and COPII vesicles (sec31) for ER exit sites in HCT116 and HCT116+A1309 cells and found that expression of truncated APC shows increased colocalization of the Golgi apparatus and COPII compared to HCT116 (Fig. 7B). Thus, truncated APC-induced Golgi fragmentation eliminates the spatial distinction between ER and the Golgi structures, followed by impairment of ER-Golgi trafficking.

Previously, we reported that truncated APC cells have defects in SREBP2 feedback activation in response to cholesterol lowering compounds, such as TASIN-1 or simvastatin (7). Considering the direct involvement of the ER-Golgi trafficking in SREBP2 processing, we tested whether truncated APC-induced Golgi fragmentation contributes to defects in SREBP2 activation and thus TASIN-1 sensitivity. To measure SREBP's activity, a Dual-Luciferase assay was performed by transfecting DLD1/shAPC isogenic cells with a plasmid encoding firefly luciferase under the control of the sterol response element (SRE)-dependent promoter and a plasmid encoding *Renilla* luciferase driven by a constitutive thymidine kinase promoter. As shown in Fig. 7C, A900- and A1309-expressing cell lines did not exhibit SRE activation in response to cholesterol-lowering drugs TASIN-1 or simvastatin treatment. In agreement, those two cell lines did not

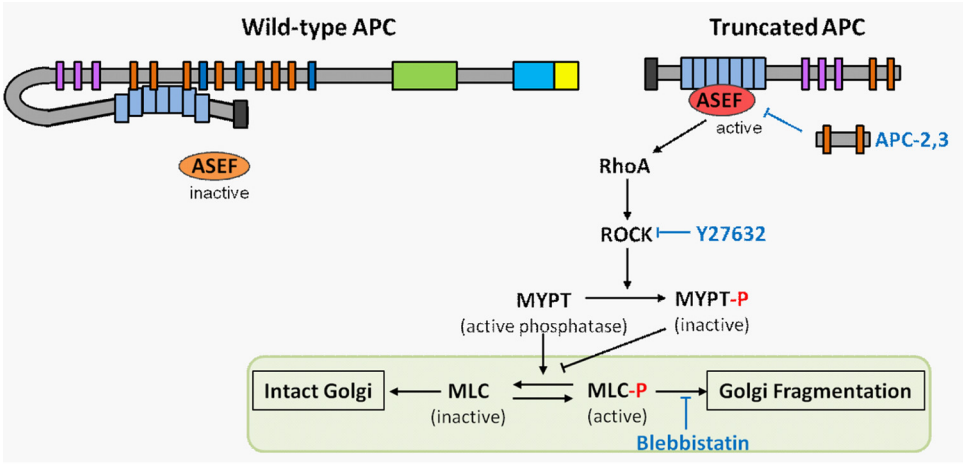

FIG 6 Models for Golgi fragmentation induced by truncated APC. Truncated APC proteins interact with Asef and activate Asef downstream signaling, resulting in activation of RhoA-ROCK-Myosin light chain II pathway and resultant Golgi fragmentation. In WT APC cells, the armadillo repeats interact with the APC-2,3 region, competing off its interaction with Asef and inactivating downstream signaling pathway, thus maintaining an intact Golgi structure.

increase expression of SREBP2 target genes similar to DLD1 cells (Fig. 7D, G, and H), while DLD1/shAPC- and A400-expressing cells showed increases in SRE activity (Fig. 7C) and expression of SREBP2 target gene in response to cholesterol lowering drugs (Fig. 7E and F). While expression of SREBP2's target genes was not increased in DLD1 cells even in serum-depleted conditions, expression of its target genes was increased in DLD1/shAPC or DLD1/APC-2,3 cells, which have intact Golgi structures (Fig. 7I to K). In addition to an increase in SREBP2 processing and expression of SREBP2's target genes, biosynthesis of cholesterol was increased in DLD1/shAPC cells compared to DLD1 cell or DLD1/shAPC+A1309 cells in serum-free conditions (Fig. 7L). These data can be interpreted to suggest that truncated APC-induced Golgi fragmentation strongly correlates with cholesterol homeostasis.

Next, we tested Golgi structure-dependent cellular responses against cholesterol lowering drug, TASIN-1. DLD1/shAPC cells with A900 and A1309 expression, which had fragmented Golgi structures, were sensitive to TASIN-1 compared to DLD1/shAPC- or A400-expressing cells (Fig. 8A). In addition, DLD1 cells expressing the APC-2,3 fragment, which had intact Golgi structures, were more resistant to TASIN-1 than DLD1 control cells (Fig. 8B). Moreover, cotreatment with blebbistatin or ROCK inhibitor conferred resistance to TASIN-1 in DLD1 (Fig. 6C).

DISCUSSION

There are several known molecular mechanisms leading to Golgi fragmentation (16). Golgi organization can be regulated by the coordination of microtubule dynamics and DNA damage responses (4, 5, 27). However, truncated APC did not induce significant microtubule depolymerization, and the DNA-PK inhibitor (NU7026) did not restore Golgi structures that were fragmented by truncated APC (data not shown). Therefore, the present results demonstrate a novel mechanism that truncated APC induces Golgi fragmentation through activating the RhoA-ROCK-MLC2 pathway in an Asef-dependent manner. This effect is dominant since overexpression of truncated APC in the presence of WT APC induced Golgi fragmentation (Fig. 1C). There is a previous report showing that truncated APC can dominantly affect cell adhesion and migration accompanied by Asef (8), but the underlying mechanism has remained unclear. In the present study, we discovered that the armadillo repeat domain within the APC protein can fold back to

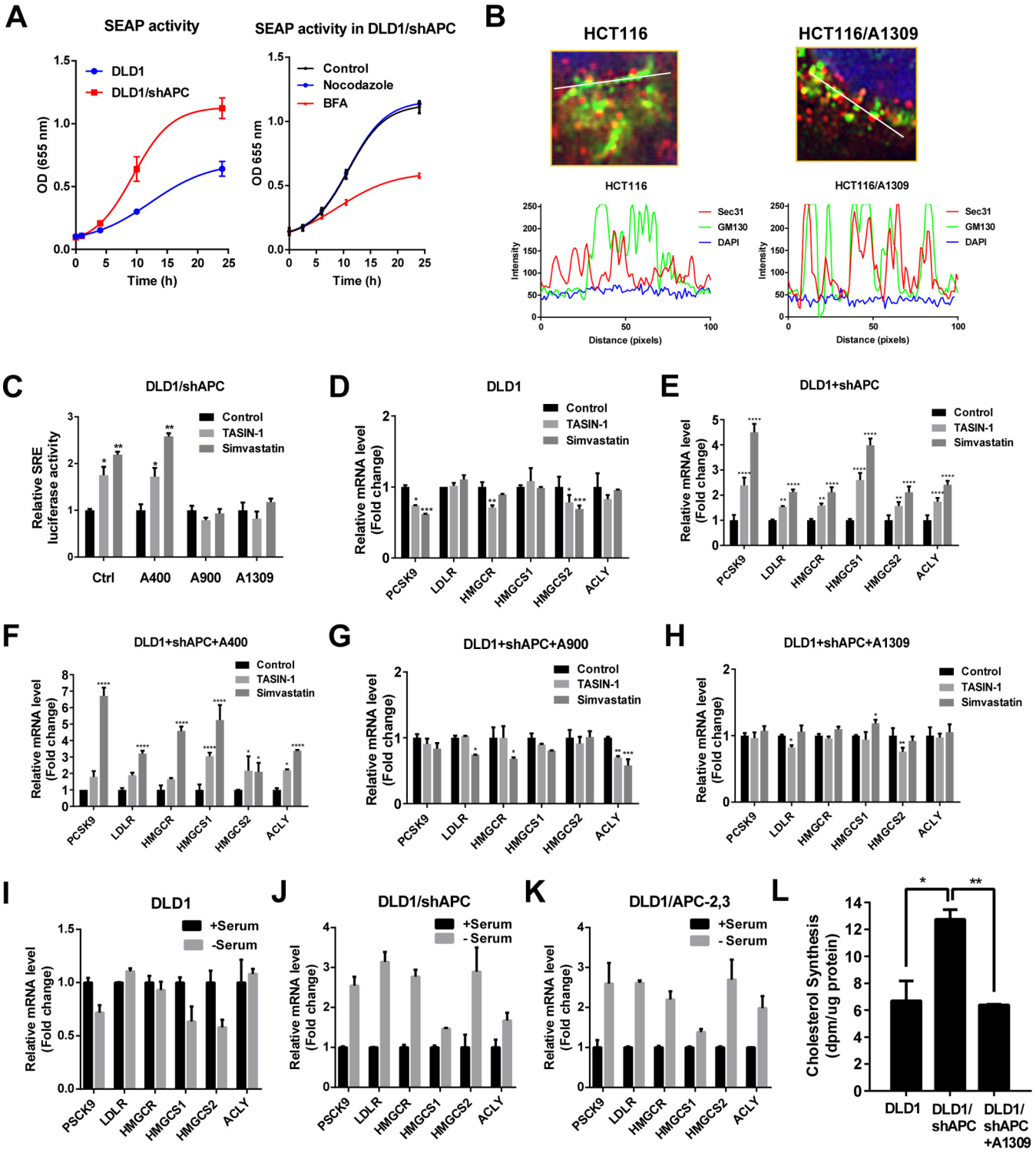

FIG 7 Fragmented Golgi structures are involved in secretory trafficking and cholesterol homeostasis. (A) DLD1 and DLD1/shAPC cells were stably transfected with pSELECT-zeo-SEAP plasmid, and the secretion of secreted embryonic alkaline phosphatase (SEAP) was monitored over time. SEAP secretion in DLD1/shAPC cells were also monitored in the presence of 1 μg/ml nocodazole or 5 μg/ml brefeldin A (BFA). (B) HCT116 and HCT116/A1309 cells were coimmunostained with Sec31 (red) and GM130 (green). RGB plot profiles illustrate the fluorescence intensity along the white line (see Fig. S7 in the supplemental material). (C) SRE promoter assay in DLD1/shAPC and its isogenic cells expressing A400, A900, and A1309 in response to 2.5 μM TASIN-1 or 5 μM simvastatin treatment for 24 h. (D to H) Quantitative RT-PCR analysis for SREBP2 target genes in DLD1 isogenic cell lines treated with or without 2.5 μM TASIN-1 or 5 μM simvastatin for 24 h. (I to K) Quantitative RT-PCR analysis for SREBP2 target genes in DLD1 (I), DLD1/shAPC (J), and DLD1/APC-2,3 (K) cell lines after incubation in low-serum media (−Serum) for 18 h. mRNA expression levels in low-serum media were normalized with the levels in high-serum media (+Serum) in each cell type. (L) Biosynthesis of cholesterol was measured using ^{14}C-labeled acetate (7) in DLD1, DLD1/shAPC, and DLD1/shAPC+A1309 cells under low-serum conditions (0.2% serum).

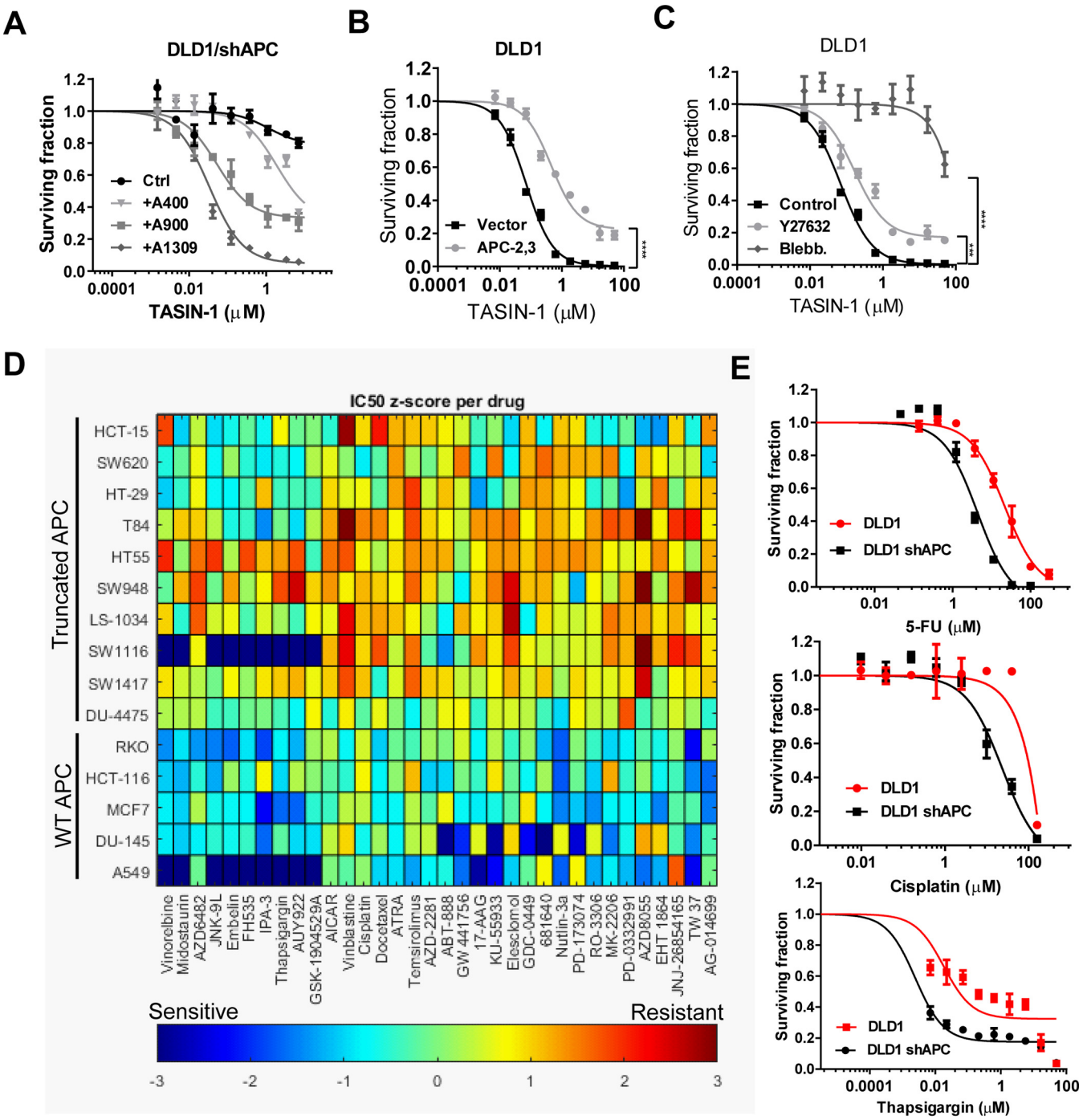

FIG 8 Effect of Golgi fragmentation in drug response. (A to C) Dose-response curves of TASIN-1 for DLD1/shAPC cells expressing different APC fragments (A), DLD1 cells with or without APC-2,3 fragment expression (B), and DLD1 cells treated with vehicle, 10 μM Y27632, or 50 μM blebbistatin (C). (D) Heatmap for drug sensitivity of various cell lines. Truncated APC cells are more resistant to 34 U.S. Food and Drug Administration-approved chemotherapy drugs compared to WT APC cells. The heatmap was made using the GDSC database (www.cancerrxgene.org). (E) Drug sensitivity of DLD1 and DLD1/shAPC cells in 5-FU, cisplatin, or thapsigargin.

interact with the APC-2,3 repeats, which disrupts its interaction with Asef, and potentially other binding partners. In support of this result, overexpression of APC-2,3 in truncated APC CRC cells mimicked the WT APC cell phenotype with regard to Golgi structure through the RhoA-ROCK-MLC2 pathway (Fig. 5G to I). This intramolecular interaction provides a possible explanation for the dominant effects of truncated APC on multiple cellular processes, but the direct contributing effector proteins other than Asef remain to be determined.

Intestinal epithelium is the most rapidly regenerating tissue in the body, with a renewal process that requires synchronized cell proliferation, migration, differentiation, and apoptosis. Colonic epithelial cell polarity and directional migration which occurs from the proliferative compartment toward the crypt collar are critical to maintain homeostasis. This upward migration and the ensuing cells shedding into the lumen provide a potential mechanism of protection to remove the cells with acquired oncogenic mutations (28). In contrast, decreased cell polarity and normal migration may permit those cells to propagate in the crypt, facilitating CRC initiation and progression (29). It is known that Golgi fragmentation results in loss of cell polarity and inhibition of directional cell migration (30). Therefore, truncated APC-induced Golgi fragmentation may be one of the earliest events that confer the selective advantage of truncated APC cells in CRC development by affecting normal directed cell migration.

This study also provides mechanistic support that Golgi fragmentation may cause defects in SREBP feedback pathway. In the context of cancer development, a decreased SREBP pathway may be a survival tactic that the cancer cells employ under stressful conditions of limited nutrients or genotoxicity in the tissue microenvironment. A previous study showing that fragmented Golgi structures provide a survival advantage for cancer cells in a genotoxic stressful condition (15) supports this hypothesis. Going forward, fragmented Golgi structures may be used as a clinical biomarker to predict sensitivity to the newly identified targeted therapeutic agent toward truncated APC cells (7) or more generally to cholesterol-lowering drugs. However, additional investigations using CRC patient samples would be necessary to validate its clinical significance as a biomarker. Fragmented Golgi is also associated with drug resistance. Investigation into the drug sensitivity databases revealed that WT APC CRC cells are relatively more sensitive to a collection of anticancer compounds compared to truncated APC CRC cells (Fig. 8D). In agreement, knockdown of truncated APC in DLD1 cells conferred drug sensitivity to 5-fluorouracil (5-FU), cisplatin, and thapsigargin (Fig. 8E). These observations also support a previous study showing that disruption of Golgi organization confers resistance to DNA-damaging agents and irradiation (15). Therefore, Golgi fragmentation may confer a cell survival advantage when cells are exposed to various forms of cellular stressors at the early stages of tumor initiation.

In conclusion, this study reveals a novel role of truncated APC in regulating Golgi structure and the underlying molecular mechanisms involved in Golgi fragmentation. Golgi fragmentation may be one of cellular events downstream of truncating APC mutation, which promotes cancer initiation and progression by providing a survival advantage for cancer cells under conditions of cellular stressors, such as DNA damage. The autoinhibition mechanism of WT APC discovered in this study provides an explanation for the dominant effects of truncated APC in promoting CRC tumorigenic properties. These findings represent a previously underappreciated function of truncated APC in cancer biology and its implications in CRC development, thus advancing our understanding of APC biology and opening up the possibility of utilizing Golgi "normalization" as a novel therapeutic strategy to sensitize CRC cells to anticancer drugs.

MATERIALS AND METHODS

Cell culture. Human colorectal cancer cell lines (DLD1, HCT116, RKO, and HT29) were obtained from American Type Culture Collection and maintained in basal medium (4 parts Dulbecco modified essential medium and 1 part M199; HyClone) supplemented with 10% cosmic calf serum. These cells were also adapted to grow in low (0.2%) serum in HCEC medium for experimental drug treatments (6). All cell lines were expanded at low passages and preserved in liquid nitrogen. Mycoplasma contamination was tested by us using an e-Myco PLUS mycoplasma PCR detection kit (Fisher Scientific).

Immunocytochemistry. Immunocytochemistry was performed as described previously (31) with minor modifications. Briefly, cells were fixed using 4.0% paraformaldehyde for 10 min, permeabilized with 0.5% Triton X-100 (TX-100) in phosphate-buffered saline (PBS) on ice for 5 min, and incubated with blocking solution (10% goat serum and 3% bovine serum albumin in PBS containing 0.1% TX-100) for 30 min. Cells were then incubated with primary antibodies diluted in PBS containing 0.1% TX-100 for an hour. Anti-GM130 antibody (610822; BD Bioscience) was used to identify the Golgi structure. After incubation with secondary antibodies labeled with Alexa Fluor 488 or Alexa Fluor 568 (Invitrogen), slides were mounted with Mowiol (Calbiochem) solution. Cells were observed under an Axiovert 200M

fluorescence microscope (Carl Zeiss). Nuclei were counterstained with DAPI (4′,6-diamidino-2-phenylindole; Vectashield; Vector Laboratories).

Recombinant proteins and pulldown assay. The coding sequence of human APC armadillo repeat (residues 407 to 775) was amplified by PCR and then cloned into a pET-28a-derived vector to be expressed as a His-tagged APC-ARM protein. Recombinant APC-ARM protein was expressed and purified as described previously (32). The APC sequence from residues 1362 to 1540, which contains the second and third 20-amino-acid repeats (APC-2,3), was amplified by PCR and then cloned into pGEX-6p vector to be expressed as a GST-tagged APC-2,3 protein. Recombinant APC-2,3 protein was expressed and purified as described previously (33). Biotin-tagged Asef-APC binding region (ABR) (biotin-HHYSHPGGGGEQLAINELISD) peptides were synthesized (KareBay Biochem, Inc.). For the pulldown assay, 40 pmol of APC-ARM and APC-2,3 were added in 50 μl of pulldown buffer (20 mM Tris-HCl [pH 7.5], 200 mM NaCl, 20 mM dithiothreitol, 0.25% NP-40, protease inhibitors) for 2 h. Then, 450 μl of pulldown buffer containing glutathione-agarose (16100; Thermo Scientific) was added for 1 h. For the *in vitro* binding competition assay, 40 pmol of APC-ARM and 200 pmol of biotin-Asef (ABR) peptide were incubated with either 40 or 80 pmol of APC-2,3 protein in 50 μl of pulldown buffer for 2 h. Biotin-Asef (ABR) was pulled down using NeutrAvidin agarose resin (29202; Thermo Scientific) in 450 μl of pulldown buffer for 1 h.

Asef pulldown and activity assay. Transiently transfected cells were harvested in ice-cold lysis buffer containing 20 mM Tris-HCl (pH 7.4), 150 mM NaCl, 0.5% TX-100, and protease inhibitor cocktail (Roche). Cell lysates were further incubated with RFP-Trap_MA (rtma-20; Chromotek) to pull down mCherry-Asef or RhoA-G17A–agarose (ab211183; Abcam) to pull down active Asef for 1 h. The beads were washed three times with lysis buffer and resuspended in 1$\times$ Laemmli sample buffer.

Sequence alignment and structure modeling. The sequence alignments of multiple species for β-catenin-ARM and APC-ARM were made using promals3D servers (34). The alignment between the β-catenin-ARM and the APC-ARM were made by Dali pairwise comparison (35) between the human β-catenin structure (1th1) and the human APC structure (3mnz). The tandem repeats in ARM domains generated multiple possible structural alignments in Dali comparison. We selected the best alignment that maximizes the overlapping of common substrate binding pockets of the ARM domain. To model the APC-2,3 binding surface for APC-ARM, we used the human β-catenin structure that binds APC-2,3 (1th1) as the structure template and replaced the β-catenin-ARM in the template with the APC-ARM (3mnz chain-A) based on the Dali alignment. APC-2,3 interaction residues were defined as those within 4 Å of the APC-2,3 peptide.

Drug sensitivity assay. Cells were seeded in 96-well plates in triplicate at a density of 3,000 or 5,000 cells/well in HCEC medium supplemented with 0.2% fetal bovine serum and treated with TASIN-1 at a 9-point 3-fold dilution series for 72 h in the presence or absence of different inhibitors, including blebbistatin (25 or 50 μM; Sigma), ROCK inhibitor (10 μM, Y-27632; Enzo Life Sciences), and MRCK inhibitor (10 μM, BDP5290; AOBIOUS, Inc.). Cell viability was determined using the CellTiter-Glo (Promega) assay according to the manufacturer's instruction. Each value was normalized to cells treated with dimethyl sulfoxide, and the 50% inhibitory concentrations were calculated using GraphPad Prism software.

siRNAs and shRNAs. We transfected 100 nM pooled siAsef (M-008235-01-0005; Dharmacon), siMLC2 (M-019044-02-0005; Dharmacon), or siControl (D001206; Dharmacon) into DLD1 cells using RNAiMAX (Invitrogen) according to the manufacturer's instructions. To establish a stable Asef knockdown cell line, DLD1 cells were infected with a lentivirus expressing an shRNA against Asef (172-0057-A-5 and 172-0378-A-8; Open Biosystems, Huntsville, AL) in the presence of 2 μg/ml Polybrene (Sigma, St. Louis, MO).

SRE promoter assay. Cells were transfected with 200 ng of pSRE-firefly luciferase and 200 ng of pTK *Renilla* luciferase plasmids in medium with 10% serum. After 24 h, the cells were replaced with HCEC media (36) containing 0.2% serum with or without 2.5 μM TASIN-1 or 5 μM simvastatin (7). The luciferase activity was measured using a Dual-Luciferase assay kit (Promega) 24 h later.

Organoid culture of patient-derived xenograft (PDX) tumor. PDX samples were initially implanted in NOD/SCID mice and harvested when the tumor reached around 2 cm in diameter. For organoid culture, tumor cells were digested, isolated, and embedded in Matrigel (1,000 single cells per 30 μl of Matrigel in 48-well plates) as described previously (37).

Quantitative RT-PCR. Total RNA was extracted by using an RNeasy minikit (Qiagen), and 1 μg of RNA was subjected to reverse transcription using a First Strand cDNA synthesis kit (Roche Molecular Biochemicals). The mRNA levels were measured by quantitative reverse transcription-PCR (RT-PCR) using SsoFast EvaGreen Supermix (Bio-Rad), and the relative expression of each gene transcript was calculated and normalized to the GAPDH transcript level.

SEAP secretion assay. Stable cell lines were established by introducing pSELECT-zeo-SEAP plasmid (psetz-seap; InvivoGen), followed by zeocin selection. Cells in 96-well plates were grown in HEK-Blue detection medium (hb-dec2; InvivoGen) and monitored via SEAP secretion. HEK-Blue Detection changes to a purple/blue color in the presence of SEAP activity. Color change can be measured by the absorbance at 566 nm (i.e., the optical density at 655 nm).

Golgi image analysis tool. In order to quantify the Golgi phenotype characteristics in cells of different treatment groups, an open-source Golgi image analysis tool was developed in MATLAB (Mathworks, Inc.). Using this GUI-based analysis tool, a user can choose a series of immunofluorescence microscopic images belonging to the same treatment group at once and crop subset images from them. A user is advised to select cropping areas carefully so that all cropped images contain only one cell each and represent overall cell phenotypes relevant to the treatment group. Only the green channel is extracted from the cropped images and used for further analysis. Therefore, the Golgi structure should be stained or changed to a green color. Each cropped image is preprocessed using the contrast-limited

adaptive histogram equalization algorithm (38) for correcting unevenly distributed background intensity. Then, the Golgi areas are detected by applying an optimal threshold calculated from a multilevel threshold algorithm, a variation of Otsu's method (39). We selected a number of fragmented areas, the sizes of the areas, and the center-to-center distances among the areas as features surrogating cell phenotypes. They are calculated for each cell and are then accumulated over all the cropped cells. As the final quantification results for the treatment group, the analysis tool returns features' histograms and statistics (means ± standard deviations). The Golgi analysis tool used in this study is available from the authors on request.

SUPPLEMENTAL MATERIAL

Supplemental material for this article may be found at https://doi.org/10.1128/MCB.00135-18.

SUPPLEMENTAL FILE 1, PDF file, 0.5 MB.

ACKNOWLEDGMENTS

We thank Joachim Seemann and Peter Michaely (UT Southwestern Medical Center, Dallas, TX) for valuable discussions. Patient-derived CRC tumors were kindly provided by Patrick Reynolds (Texas Tech University Health Sciences Center, Lubbock, Texas). Plasmids for mCherry-Asef FL and Asef(Δ270) were kindly provided by Kent Rossman (UNC Lineberger Comprehensive Cancer Center, Chapel Hill, NC). Plasmids for GFP-tagged APC fragments were kindly provided by Beric R. Henderson (Westmead Millennium Institute at Westmead Hospital, Wesmead, New South Wales, Australia) and Mariann Bienz (Laboratory of Molecular Biology, Hills Road, Cambridge, UK).

Y.-A.M. is supported by an international cooperation program managed by National Research Foundation of Korea (NRF-2015K2A1A2069549), and S.B.K. is supported by Brain Pool program funded by the Ministry of Science and ICT through the National Research Foundation of Korea (grant 2018H1D3A2000524). This study was supported by CPRIT grants RP130189 and RP160180 to J.W.S. This study was performed in laboratories constructed with support from NIH grant C06RR30414.

There is no conflict of interest.

REFERENCES

1. Fearnhead NS, Britton MP, Bodmer WF. 2001. The ABC of APC. Hum Mol Genet 10:721–733. https://doi.org/10.1093/hmg/10.7.721.
2. Bienz M, Clevers H. 2000. Linking colorectal cancer to Wnt signaling. Cell 103:311–320. https://doi.org/10.1016/S0092-8674(00)00122-7.
3. Miyoshi Y, Nagase H, Ando H, Horii A, Ichii S, Nakatsuru S, Aoki T, Miki Y, Mori T, Nakamura Y. 1992. Somatic mutations of the APC gene in colorectal tumors: mutation cluster region in the APC gene. Hum Mol Genet 1:229–233. https://doi.org/10.1093/hmg/1.4.229.
4. Juanes MA, Bouguenina H, Eskin JA, Jaiswal R, Badache A, Goode BL. 2017. Adenomatous polyposis coli nucleates actin assembly to drive cell migration and microtubule-induced focal adhesion turnover. J Cell Biol 216:2859–2875. https://doi.org/10.1083/jcb.201702007.
5. Mimori-Kiyosue Y, Shiina N, Tsukita S. 2000. Adenomatous polyposis coli (APC) protein moves along microtubules and concentrates at their growing ends in epithelial cells. J Cell Biol 148:505–518. https://doi.org/10.1083/jcb.148.3.505.
6. Mogensen MM, Tucker JB, Mackie JB, Prescott AR, Nathke IS. 2002. The adenomatous polyposis coli protein unambiguously localizes to microtubule plus ends and is involved in establishing parallel arrays of microtubule bundles in highly polarized epithelial cells. J Cell Biol 157:1041–1048. https://doi.org/10.1083/jcb.200203001.
7. Zhang L, Theodoropoulos PC, Eskiocak U, Wang W, Moon YA, Posner B, Williams NS, Wright WE, Kim SB, Nijhawan D, De Brabander JK, Shay JW. 2016. Selective targeting of mutant adenomatous polyposis coli (APC) in colorectal cancer. Sci Transl Med 8:361ra140. https://doi.org/10.1126/scitranslmed.aaf8127.
8. Kawasaki Y, Sato R, Akiyama T. 2003. Mutated APC and Asef are involved in the migration of colorectal tumour cells. Nat Cell Biol 5:211–215. https://doi.org/10.1038/ncb937.
9. Green RA, Kaplan KB. 2003. Chromosome instability in colorectal tumor cells is associated with defects in microtubule plus-end attachments caused by a dominant mutation in APC. J Cell Biol 163:949–961. https://doi.org/10.1083/jcb.200307070.
10. Brocardo M, Lei Y, Tighe A, Taylor SS, Mok MT, Henderson BR. 2008. Mitochondrial targeting of adenomatous polyposis coli protein is stimulated by truncating cancer mutations: regulation of Bcl-2 and implications for cell survival. J Biol Chem 283:5950–5959. https://doi.org/10.1074/jbc.M708775200.
11. Nelson SA, Li Z, Newton IP, Fraser D, Milne RE, Martin DM, Schiffmann D, Yang X, Dormann D, Weijer CJ, Appleton PL, Nathke IS. 2012. Tumorigenic fragments of APC cause dominant defects in directional cell migration in multiple model systems. Dis Model Mech 5:940–947. https://doi.org/10.1242/dmm.008607.
12. Kawasaki Y, Senda T, Ishidate T, Koyama R, Morishita T, Iwayama Y, Higuchi O, Akiyama T. 2000. Asef, a link between the tumor suppressor APC and G-protein signaling. Science 289:1194–1197. https://doi.org/10.1126/science.289.5482.1194.
13. Jiang H, Deng R, Yang X, Shang J, Lu S, Zhao Y, Song K, Liu X, Zhang Q, Chen Y, Chinn YE, Wu G, Li J, Chen G, Yu J, Zhang J. 2017. Peptidomimetic inhibitors of APC-Asef interaction block colorectal cancer migration. Nat Chem Biol 13:994–1001. https://doi.org/10.1038/nchembio.2442.
14. Xing M, Peterman MC, Davis RL, Oegema K, Shiau AK, Field SJ. 2016. GOLPH3 drives cell migration by promoting Golgi reorientation and directional trafficking to the leading edge. Mol Biol Cell 27:3828–3840. https://doi.org/10.1091/mbc.e16-01-0005.
15. Farber-Katz SE, Dippold HC, Buschman MD, Peterman MC, Xing M, Noakes CJ, Tat J, Ng MM, Rahajeng J, Cowan DM, Fuchs GJ, Zhou H, Field SJ. 2014. DNA damage triggers Golgi dispersal via DNA-PK and GOLPH3. Cell 156:413–427. https://doi.org/10.1016/j.cell.2013.12.023.
16. Petrosyan A. 2015. Onco-Golgi: is fragmentation a gate to cancer progression? Biochem Mol Biol J 1:16.
17. Brown MS, Goldstein JL. 1997. The SREBP pathway: regulation of cho-

lesterol metabolism by proteolysis of a membrane-bound transcription factor. Cell 89:331–340. https://doi.org/10.1016/S0092-8674(00)80213-5.
18. Horton JD, Goldstein JL, Brown MS. 2002. SREBPs: activators of the complete program of cholesterol and fatty acid synthesis in the liver. J Clin Invest 109:1125–1131. https://doi.org/10.1172/JCI0215593.
19. Hinoi T, Akyol A, Theisen BK, Ferguson DO, Greenson JK, Williams BO, Cho KR, Fearon ER. 2007. Mouse model of colonic adenoma-carcinoma progression based on somatic APC inactivation. Cancer Res 67:9721–9730. https://doi.org/10.1158/0008-5472.CAN-07-2735.
20. Zhang Z, Chen L, Gao L, Lin K, Zhu L, Lu Y, Shi X, Gao Y, Zhou J, Xu P, Zhang J, Wu G. 2012. Structural basis for the recognition of Asef by adenomatous polyposis coli. Cell Res 22:372–386. https://doi.org/10.1038/cr.2011.119.
21. Watanabe T, Wang S, Noritake J, Sato K, Fukata M, Takefuji M, Nakagawa M, Izumi N, Akiyama T, Kaibuchi K. 2004. Interaction with IQGAP1 links APC to Rac1, Cdc42, and actin filaments during cell polarization and migration. Dev Cell 7:871–883. https://doi.org/10.1016/j.devcel.2004.10.017.
22. Sudhaharan T, Goh WI, Sem KP, Lim KB, Bu W, Ahmed S. 2011. Rho GTPase Cdc42 is a direct interacting partner of adenomatous polyposis coli protein and can alter its cellular localization. PLoS One 6:e16603. https://doi.org/10.1371/journal.pone.0016603.
23. Mitin N, Betts L, Yohe ME, Der CJ, Sondek J, Rossman KL. 2007. Release of autoinhibition of ASEF by APC leads to CDC42 activation and tumor suppression. Nat Struct Mol Biol 14:814–823. https://doi.org/10.1038/nsmb1290.
24. Wilkinson S, Paterson HF, Marshall CJ. 2005. Cdc42-MRCK and Rho-ROCK signaling cooperate in myosin phosphorylation and cell invasion. Nat Cell Biol 7:255–261. https://doi.org/10.1038/ncb1230.
25. Petrosyan A, Holzapfel MS, Muirhead DE, Cheng PW. 2014. Restoration of compact Golgi morphology in advanced prostate cancer enhances susceptibility to galectin-1-induced apoptosis by modifying mucin O-glycan synthesis. Mol Cancer Res 12:1704–1716. https://doi.org/10.1158/1541-7786.MCR-14-0291-T.
26. Xing Y, Clements WK, Le Trong I, Hinds TR, Stenkamp R, Kimelman D, Xu W. 2004. Crystal structure of a beta-catenin/APC complex reveals a critical role for APC phosphorylation in APC function. Mol Cell 15:523–533. https://doi.org/10.1016/j.molcel.2004.08.001.
27. Copeland SJ, Thurston SF, Copeland JW. 2016. Actin- and microtubule-dependent regulation of Golgi morphology by FHDC1. Mol Biol Cell 27:260–276. https://doi.org/10.1091/mbc.e15-02-0070.
28. Dunn SJ, Nathke IS, Osborne JM. 2013. Computational models reveal a passive mechanism for cell migration in the crypt. PLoS One 8:e80516. https://doi.org/10.1371/journal.pone.0080516.
29. Nathke IS. 2004. The adenomatous polyposis coli protein: the Achilles heel of the gut epithelium. Annu Rev Cell Dev Biol 20:337–366. https://doi.org/10.1146/annurev.cellbio.20.012103.094541.
30. Yadav S, Puri S, Linstedt AD. 2009. A primary role for Golgi positioning in directed secretion, cell polarity, and wound healing. Mol Biol Cell 20:1728–1736. https://doi.org/10.1091/mbc.e08-10-1077.
31. Roig AI, Hight SK, Shay JW. 2009. Two- and three-dimensional models for risk assessment of radiation-enhanced colorectal tumorigenesis. Radiat Res 171:33–40. https://doi.org/10.1667/RR1415.1.
32. Zhang Z, Lin K, Gao L, Chen L, Shi X, Wu G. 2011. Crystal structure of the armadillo repeat domain of adenomatous polyposis coli which reveals its inherent flexibility. Biochem Biophys Res Commun 412:732–736. https://doi.org/10.1016/j.bbrc.2011.08.044.
33. Xing Y, Clements WK, Kimelman D, Xu W. 2003. Crystal structure of a beta-catenin/axin complex suggests a mechanism for the beta-catenin destruction complex. Genes Dev 17:2753–2764. https://doi.org/10.1101/gad.1142603.
34. Pei J, Grishin NV. 2014. PROMALS3D: multiple protein sequence alignment enhanced with evolutionary and three-dimensional structural information. Methods Mol Biol 1079:263–271. https://doi.org/10.1007/978-1-62703-646-7_17.
35. Hasegawa H, Holm L. 2009. Advances and pitfalls of protein structural alignment. Curr Opin Struct Biol 19:341–348. https://doi.org/10.1016/j.sbi.2009.04.003.
36. Roig AI, Eskiocak U, Hight SK, Kim SB, Delgado O, Souza RF, Spechler SJ, Wright WE, Shay JW. 2010. Immortalized epithelial cells derived from human colon biopsies express stem cell markers and differentiate in vitro. Gastroenterology 138:1012–1021. https://doi.org/10.1053/j.gastro.2009.11.052.
37. Sato T, Stange DE, Ferrante M, Vries RG, Van Es JH, Van den Brink S, Van Houdt WJ, Pronk A, Van Gorp J, Siersema PD, Clevers H. 2011. Long-term expansion of epithelial organoids from human colon, adenoma, adenocarcinoma, and Barrett's epithelium. Gastroenterology 141:1762–1772. https://doi.org/10.1053/j.gastro.2011.07.050.
38. Pizer SM, Amburn EP, Austin JD, Cromatie R, Geselowitz A, Greer T, Zuiderveld K. 1987. Adaptive histogram equalization and its variations. Computer vision, graphics, and image processing 39:355–368. https://doi.org/10.1016/S0734-189X(87)80186-X.
39. Liao PS, Chen TS, Chung PC. 2001. A fast algorithm for multilevel thresholding. J Infect Sci Eng 17:713–727.